Experiments on the synchronous sloshing in suspended containers described by shallow-water theory.

Patrick Weidman
Department of Mechanical Engineering
University of Colorado
Boulder, CO 80309-0427
USA

M. R. Turner
Department of Mathematics
University of Surrey
Guildford, Surrey GU2 7XH
UK

Abstract

The synchronous interaction between a sloshing fluid and its container may take place when the motion of the container is not prescribed *a priori*. When a partially-filled container is suspended as a bifilar pendulum, the fluid contributes to the restoring force by its weight through the wire suspensions and may either augment or diminish the restoring force through hydrodynamic interaction with the container. Here we report on linearized shallow-water theory and experiments for multi-chamber box containers, a cylinder and an upright 90° wedge. The nature of system response at low fluid mass is analyzed in detail using linear theory and shallow-water simulations. These results show that the system frequency smoothly transitions through successive higher frequency eigenmodes so that, in the limit where the fluid mass tends to zero, the system frequency is that of the dry container.

1 Introduction

The dynamics of containers partially-filled with liquid dates back to the classical work of nineteenth-century scientists. In the mid-twentieth century, interest in such problems was revived owing to a number of technical applications ranging from seismic oscillations of fuel reservoirs to the dynamics of aircraft and rockets taking into account fuel which they carry. These problems are distinct from the problem of fluid oscillations brought about by a prescribed motion of the container: in the unconstrained or partially constrained problems of interest here the motion of the container depends crucially on the dynamics of the fluid within. A theory for the oscillations of a beam with a liquid-containing cavity was reported by Moiseev (1964) and other problems of this type related to space vehicle technology may be found in a NASA publication edited by Abramson (1966).

An article by Cooker (1994) considers the interesting problem of fluid-container interaction when the container is suspended as a bifilar pendulum with equal suspension lengths l. For small nondimensional displacements X_0/l of the pendulum about equilibrium, the motion is close to being horizontal only, with the vertical deflection of the container being of order $(X_0/l)^2$. The natural oscillation frequency for a dry container is the pendulum frequency $\omega_0 = \sqrt{g/l}$, where g is the gravitational constant. Cooker's experiments performed with a container partially filled with water and released away from equilibrium showed that large amplitude waves are generated at the sidewall during the first swing. These waves dissipate with each subsequent swing and eventually the system settles down to periodic motion at frequency $\omega_1 < \omega_0$, with the fluid moving synchronously in-phase with the pendulum. Other initial conditions gave synchronous fluid motion exactly out-of-phase with the pendulum in which case the system oscillated at frequency $\widehat{\omega}_1$, such that $\omega_1 < \widehat{\omega}_1$.

Cooker (1994) formulated two problems, each helping to understand the above observations. In the first, two-dimensional linearized shallow-water theory was employed to analyze how sloshing motions in a tank of uniform rectangular cross-section interact with the gravitational restoring force to give a discrete spectrum of wave modes synchronized with the motion of the container. A transcendental equation obtained for the wavenumber of fluid sloshing was solved numerically using Newton iteration. Results for the fundamental frequency of in-phase motion were shown to be in accord with the seiche frequency observed in experiments. In the second problem, linearized potential theory with the hydrostatic pressure assumption was used to find planar geometries admitting synchronous solutions for suspended containers. The container shapes uncovered were a family of hyperbolae includ-

ing, as a limiting container form, a wedge with 90° vertex angle. Both in-phase frequencies ω_1 and anti-phase frequencies $\widehat{\omega}_1$ of a planar free surface oscillating about its central nodal line were reported, and it was shown that $\omega_1 < \widehat{\omega}_1$.

It may be noted that the limit $l \to \infty$ for the pendulum supported system corresponds to the *free motion* of a fluid-filled container wherein the sole driving force is the fluid sloshing against the container walls. Potential flow theory and corresponding experiments carried out for this type of motion in boxes, cylinders, wedges, cones, and cylindrical annulii have been reported by Herczynski and Weidman (2012).

In his single-chamber calculations, Cooker (1994) reported oscillation frequencies that depend on two parameters: $G = (1 + R)D^2/lH$ and $R = m_0/m$, in which m_0 is the mass of the dry container, m the fluid mass, D the half-length of the container and H the mean fluid depth. While the dimensionless parameters G and R conveniently exhibit the graphical solution of the eigenvalue equation, they are not independent since G depends on R both explicitly and implicitly though the fluid depth H. In this paper we determine new independent parameters using dimensional analysis.

The shallow-water theory of Cooker (1994) was extended to non-shallow depth fluids by Yu (2010) who found that in this scenario the rectangular and cylindrical container eigenmodes consist of the shallow-water eigenmode plus a sum of vertical eigenmodes (Linton and McIver, 2001). Results were presented showing the dramatic effect of finite, but non-shallow, fluid depths. Alemi Ardakani *et al.* (2012) found that the rectangular container can exhibit a 'resonance' behaviour, where anti-symmetric fluid eigenmodes, which couple to the vessel motion, can have the same oscillation frequency as the symmetric fluid eigenmodes, which exhibit zero force on the container. These ideas were also examined for multi-chamber rectangular containers in Turner *et al.* (2013).

In the present investigation it is assumed that each container examined is suspended as a bifilar pendulum and we consider fluid depths for which the motion may be adequately modelled using shallow-water theory. An exception is the motion of a 90° wedge for which shallow-water theory does not apply. In this case we derive the oscillation frequency of the wedge suspended as a bifilar pendulum using potential theory. Also we focus on in-phase sloshing motions which are readily obtained in laboratory experiments by simply pulling back the container from equilibrium and releasing it gently with the fluid initially at rest.

In §2 we extend the constant depth shallow-water analysis of Cooker (1994) for sloshing in a channel of rectangular section to a multi-chamber container suspended as a bifilar pendulum. In §3 the sideways sloshing of fluid in a vertically suspended cylindrical container is

considered in the context of linearized shallow-water theory where solutions for synchronous oscillation in terms of Bessel functions are obtained. Potential theory for the 90° wedge is presented in §4. Experimental measurements for each of the above containers are presented in §5. In §6 we present experimental results and theory for the case of small fluid-to-container mass ratios, m/m_0, showing a transition through higher frequency eigenmodes as this ratio is reduced. A discussion of results and concluding remarks are given in §7.

2 Multicompartment Containers

An interesting question of wavenumber selection arises when one considers the motion of a single container divided into different compartments partially filled with fluid and suspended as a bifilar pendulum. The situation is sketched in figure 1. The problem is solved by a straightforward extension of the shallow-water analysis given by Cooker (1994) for a single rectangular channel, but now N compartments of arbitrary length, width, and quiescent fluid depth are considered. The resulting characteristic equation for the system frequencies was first derived by Turner *et al.* (2013), but here we recreate this derivation in our notation We denote the compartment widths W_n, compartment lengths $L_n = 2D_n$, quiescent fluid depths H_n, fluid densities ρ_n, compartment fluid masses $m_n = \rho_n W_n L_n H_n$, and the fixed container mass is m_0.

The fluid motion in each compartment is assumed to be governed by the linear, shallow-water equations

$$\frac{\partial \eta_n}{\partial t} = -H\frac{\partial u_n}{\partial x}, \qquad \frac{\partial u_n}{\partial t} = -g\frac{\partial \eta_n}{\partial x} \tag{2.1}$$

where u_n is the absolute horizontal velocity of the fluid, independent of the depth in the shallow-water approximation, η_n is the free surface displacement, x is a horizontal space coordinate in the moving frame, measured from the center of the container and t is time.

Solutions are sought for which the container moves in simple harmonic motion according to

$$X(t) = X_0 \cos \omega t \tag{2.2}$$

where ω is the container angular frequency and X_0 is the maximum horizontal displacement of the container from equilibrium. We use a frame of reference moving with the container centered at the free surface so the bottom wall lies at $z = -H$. Realizing that ω is the sole eigenvalue to be determined for any multi-compartment container, we write the linearized free surface disturbances $\eta_n(x, t)$ satisfying Eqs. (2.1) in each compartment in terms of the

frequency as

$$\eta_n(x,t) = X_0 \frac{H_n \omega \tau_n}{D_n \cos(\omega \tau_n)} \sin[\omega \tau_n (x/D_n)] \cos \omega t \tag{2.3}$$

where $\tau_n = D_n/\sqrt{g\,H_n}$ are characteristic compartment periods. This solution satisfies the sidewall boundary conditions $u_n(\pm D, t) = \dot{X}$. The wavenumbers κ_n selected by each compartment are given by

$$\kappa_n = \frac{2\pi}{\lambda_n} = \frac{\omega}{\sqrt{g\,H_n}} \tag{2.4}$$

where λ_n are the disturbance wavelengths. It may be recalled (Stoker, 1957) that terms neglected in the shallow-water derivation are of order $\delta = (H/\lambda)^2$ and terms neglected in its linearization are of order $\epsilon = \eta_0/H$, where η_0 is the maximum amplitude of the disturbance. Hence any results derived from application of (2.2) are restricted to $\delta \ll 1$ and $\epsilon \ll 1$.

For small displacements of the container from equilibrium, the gravitational restoring force transmitted through the pendulum wire supports is

$$F_g = (F_g)_{m_0} + (F_g)_m = -\,\omega_0^2 m_0 X - \omega_0^2 \sum_{n=1}^{N} m_n X \tag{2.5}$$

in which $(F_g)_{m_0}$ is the contribution from the dry container and $(F_g)_m$ is the contribution from the liquid distributed through the various compartments. The net horizontal hydrostatic force acting from all compartments according to linear theory is

$$F_p = \sum_{n=1}^{N} \rho_n g H_n W_n [\eta_n] = \sum_{n=1}^{N} \frac{X_0 m_n \omega}{\tau_n} \tan(\omega \tau_n) \cos \omega t \tag{2.6}$$

where $[\eta_n]$, the difference in fluid heights at the endwalls $x = \pm D_n$ of each container, has been evaluated using (2.3). The equation of motion for the container is then

$$m_0 \ddot{X} = (F_g)_{m_0} + (F_g)_m + F_p. \tag{2.7}$$

Newton's second law in (2.7) is generic for suspended containers — only the hydrostatic pressure force F_p depends on the geometry of the compartment(s) housing the liquid. The effect of adding fluid mass to a dry container is not entirely obvious: the fluid contributes a restoring force through the term $(F_g)_m$, but F_p may be either retarding or restoring. Dividing (2.7) by m_0 and introducing the fluid/container mass ratios

$$M_n = \frac{m_n}{m_0} \tag{2.8}$$

equations (2.5), (2.6) and (2.7) yield

$$\ddot{X} + \Omega^2 X = X_0 \cos \omega t \sum_{n=1}^{N} \frac{M_n \omega}{\tau_n} \tan(\omega \tau_n) \tag{2.9}$$

where

$$\Omega^2 = \omega_0^2 \left(1 + \sum_{n=1}^{N} M_n \right). \tag{2.10}$$

Clearly $\Omega > \omega_0$ whenever there is any fluid present; for this reason Ω will henceforth be called the *fluid-augmented pendulum frequency*. The fluid does not actually slosh at this frequency, but it will be shown that Ω plays an important role in determining frequency bounds for synchronous sloshing.

A major goal is to determine how the frequency of periodic motion is affected by M_n. Thus only the particular solution of (2.9) is required, assuming the length of the pendulum is such as to not cause resonance. (The reader is referred to Cooker (1994) and Turner *et al.* (2013) for a discussion of the resonance problem.) If the fluid is to move synchronously with the container, equation (2.2) must also satisfy (2.9) and this leads to the generalized transcendental eigenvalue relation

$$\omega^2 = \Omega^2 - \sum_{n=1}^{N} M_n \frac{\omega}{\tau_n} \tan(\omega \tau_n) \tag{2.11}$$

for the frequency of the suspended container. It can be shown that this agrees with the term in brackets in (5.1) of Turner *et al.* (2013).

For the fundamental seiche mode $0 < \omega_1 \tau_n < \pi/2$ and each term under the summation sign in (2.11) is positive definite and $\tau_n \neq 0$; hence the fundamental frequency ω_1 is bounded from above by Ω. In fact, for a single compartment, Cooker (1994) has shown that $\omega_1 \leq \omega_0 \leq \Omega$.

There are various scenarios by which one could envision adding liquid mass to the compartmentalized system, and in general each scenario will yield a different oscillation frequency for the same total liquid volume, even if all liquid densities ρ_n are equal.

2.1 A new choice of parameters

Consider for the moment a single-compartment analysis so that we dispense with the $n = 1$ subscript. Eleven independent variables are identified: ω, λ, η_0, X_0, m_0, m, ρ, g, D, W, and l. Here η_0 is the maximum amplitude of the fundamental seiche motion. Since the number

of dimensions (mass, length, and time) is three, Buckingham's pi theorem (Murphy, 1950) states there will be eight independent dimensionless Π parameters here taken as

$$\frac{\omega}{\omega_0}, \quad \frac{\lambda}{2D}, \quad \frac{\eta_0}{X_0}; \qquad \frac{m}{m_0}, \quad \frac{m_0 l}{2\rho D^3 W}, \quad \frac{l}{D}, \quad \frac{W}{D}, \quad \frac{X_0}{D} \tag{2.12}$$

where $\omega_0 = \sqrt{g/l}$ and the factors of two are chosen for convenience. The first three Π terms define the state of motion and are, in general, functions of the remaining five Π terms. We denote η_0/X_0 the amplification ratio measuring the maximum *vertical* displacement of the fluid for given maximum *horizontal* displacement of the container. In addition to the obvious length ratios and the fluid/container mass ratio $M = m/m_0$, there appears the new parameter here denoted

$$\mu = \frac{m_0 l}{2\rho D^3 W}. \tag{2.13}$$

We now attempt to assign the physical significance of μ. For a free box container, the D'Alembert acceleration force $m_0\ddot{X}$ is balanced by the driving hydrodynamic pressure force F_p in Eq. (2.7). Consider a half-sine wave which just fits inside the container of length $2D$ for which $[\eta] = 2\eta_0$ and $\lambda = 4D$. Then the force balance for free motion gives

$$m_0\ddot{X} = 2\rho g H W \eta_0 = 2\rho g W D^2 \left(\frac{H\eta_0}{D^2}\right). \tag{2.14}$$

Thus the acceleration ratio is

$$\frac{g}{\ddot{X}} = \frac{m_0}{2\rho H W \eta_0} = \overline{\mu}\left(\frac{D^2}{H\eta_0}\right) \qquad \text{where} \qquad \overline{\mu} = \frac{m_0}{2\rho D^2 W}. \tag{2.15}$$

For $\lambda = \mathrm{O}(D)$ we estimate the amplitude $\epsilon = \eta_0/H$ and disperison $\delta = (H/\lambda)^2$ parameters to obtain from (2.15)

$$\overline{\mu} \sim \epsilon\delta\left(\frac{g}{\ddot{X}}\right) \tag{2.16}$$

for a free container and since $\mu = (l/D)\overline{\mu}$ we have

$$\mu \sim \epsilon\delta\left(\frac{l}{D}\right)\left(\frac{g}{\ddot{X}}\right) \tag{2.17}$$

for a suspended container. Thus μ represents the ratio of *vertical* gravitational acceleration to the *horizontal* container acceleration magnified by the pendulum length factor l/D and reduced by the product $\epsilon\delta$ where $\epsilon \ll 1$ and $\delta \ll 1$.

We note that the dimensionless parameter G used by Cooker (1994) is related to M and μ in the form

$$G \equiv \frac{(1+R)D^2}{l\,H} = \left(\frac{M+1}{M^2}\right)\mu \tag{2.18}$$

in which $R \equiv m_0/m = 1/M$. Thus, using dimensional analysis, and generalizing (2.11) to n-compartments, we are now able to write the eigenvalue equation for the oscillation frequency in terms of $2N$ independent parameters M_n and μ_n as

$$\left(\frac{\omega}{\omega_0}\right)^2 = 1 + \sum_{n=1}^{N} \left\{ M_n - \mu_n^{1/2} M_n^{3/2} \left(\frac{\omega}{\omega_0}\right) \tan\left[\frac{\omega/\omega_0}{\sqrt{\mu_n M_n}}\right] \right\} \tag{2.19}$$

where μ_n, and the dimensionless wavelengths in each chamber obtained using Eq. (2.4), are

$$\mu_n = \frac{l\, m_0}{2\rho_n D_n^3 W_n}, \qquad \frac{\lambda_n}{L_n} = \pi \frac{\sqrt{\mu_n M_n}}{\omega/\omega_0}. \tag{2.20}$$

Finally, for the fundamental seiche mode, the extreme liquid elevations $(\eta_0)_n$ occur at the endwalls $x = \pm D_n$ and careful evaluation of (2.3) then gives the compartment amplification ratios

$$\frac{(\eta_0)_n}{X_0} = \frac{D_n}{l}\sqrt{\mu_n M_n}\left(\frac{\omega}{\omega_0}\right)\tan\left(\frac{\omega/\omega_0}{\sqrt{\mu_n M_n}}\right). \tag{2.21}$$

2.2 Numerical examples

For the multi-compartment problem one has to decide how to add fluid to the system. As a first example, consider distributing a given volume of fluid of uniform density ρ to a container of mass m_0 segmented into N identical compartments of length L and width W. Let M be the total dimensionless fluid mass available. In the first instance one compartment is continuously filled with all the fluid M. Next, to see the effect of fluid distribution, two compartments are simultaneously filled, each to mass $M/2$. This process is continued to N compartments simultaneously filled to mass M/N. As an example we choose $N = 5$ compartments with $W = 0.1$ m, $L = 0.5$ m, $l = 1.0$ m, $m_0 = 1$ kg, $g = 9.80$ m/sec^2, $\rho = 1000$ kg/m^3 and a total dimensionless fluid mass $M = 7.5$. The pendulum frequency for this example is $\omega_0 = 3.130$ rad/sec and $\mu = 0.32$. The maximum fluid levels range from 3 cm for the simultaneous filling of all five compartments to 15 cm for a single compartment filling.

Numerical solutions of the eigenvalue equations reported in §§2-5 of this investigation were obtained using an IMSL root finder for nonlinear equations. Frequencies determined from (2.19) for the above five different filling procedures are shown in figure 2. Distributing the fluid to an increasing number of compartments has the effect of decreasing the (synchronous) frequency ω of the system. Note that $\omega \to \omega_0$ as $M \to \infty$. There is clearly a problem as $M \to 0$, however, because in this limit the dry container frequency ω_0 must be obtained for which $\omega/\omega_0 = 1$. This discrepancy will be addressed in §6 of the paper.

As a second example of the effect of compartmentalizing a given quantity of fluid, we consider the four different containers sketched in figure 3 which are referred to as 'boxes', 'triple', 'single', and '3deep' configurations. Each container has mass $m_0 = 1.0$ kg and width $W = 0.1$ m. The 'boxes' container is composed of three compartments of lengths $L_1 = 0.8$ m, $L_2 = 0.6$ m, and $L_3 = 0.4$ m; the 'single' container has length $L_1 = 1.8$ m; the 'triple' and '3deep' containers are of length $L_1 = 0.6$ m. For simplicity, we set the pendulum length $l = 1.0$ m and add 18 kg total fluid mass by increasing the fluid mass equally in each of the four containers; for the 'triple box the added fluid mass is distributed uniformly to each of the three compartments. The maximum fluid depth in the compartment of every configuration is 0.1 m with the exception of the '3deep' container which has maximum fluid depth of 0.3 m. We use $g = 9.80$ m/s^2 and $\rho = 1000$ kg/m^3 in the calculations reported below.

The fundamental in-phase frequencies are obtained through the solution of Eq. (2.19) for each case. The frequencies ω/ω_0 as a function of M are presented in figure 4(a). Note that all frequency curves remain distinct; *i.e.*, they share no common points, apart from the nonphysical zero oscillation frequency at $M = 0$. The 'single' box exhibits the lowest frequency and frequencies increase as one proceeds to the 'boxes', 'triple', and '3deep' configurations. The results in figure 4(a) show that the distribution of mass uniformly filling different containers has a marked effect on the oscillation frequency both at low and high values of M. In figure 4(b) the dimensionless wavelengths computed from Eq. (2.20) selected by each container are given as a function of M; all wavelengths are normalized by the longest compartment length L_1 in each configuration so that the dry box limit of each is $\lambda/L_1 = 2.0$. The wavelengths in each compartment of 'boxes' are equal as are those for the "triple" configuration. However, the compartment waveforms in 'boxes' are now distinct since the compartment amplification ratios depend on D_n, as can be seen in Eq. (2.21).

3 Cylindrical Containers

In this section the motion of a partially filled cylindrical container of radius R is studied using the shallow-water approximation. We use cylindrical polar coordinates (r, θ, z) with the origin at the center of the free surface and the z-axis directed upward antiparallel to gravity, with corresponding velocity components (u, v, w). The linearized shallow-water equations in an inertial frame are given by

$$u_t + g\eta_r = 0, \qquad v_t + \frac{g}{r}\eta_\theta = 0, \tag{3.1a, b}$$

$$\eta_t + \frac{1}{r}(ruh)_r + \frac{1}{r}(vh)_\theta = 0 \tag{3.1c}$$

where the free surface is located at $z = \eta(r, \theta, t)$ and the flat bottom of the right circular cylinder is at $z = -H$. In the shallow-water approximation (u, v) are functions of (r, θ, t) only and the pressure is hydrostatic. Elimination of u and v in (3.1c) shows that the free surface displacement is governed by the wave equation

$$\eta_{tt} = C_0^2 \left[\frac{1}{r}(r\eta_r)_r + \frac{1}{r^2}\eta_{\theta\theta}\right] \tag{3.2}$$

wherein $C_0 = \sqrt{gH}$. For sideways periodic motion $X(t) = X_0 \cos \omega t$, the linearized condition that the normal component of fluid velocity at the cylinder sidewall $r = R$ is equal the normal component of container velocity is given by

$$u(R, \theta, t) = -X_0 \omega \cos\theta \sin \omega t. \tag{3.3}$$

Guided by this boundary condition and noting from (3.1a) that η_r is proportional to u_t we look for a free surface displacement of the form

$$\eta(r, \theta, t) = f(r) \cos\theta \cos \omega t. \tag{3.4}$$

Substituting (3.4) into (3.2) and introducing $\xi = r\omega/C_0$ yields Bessel's equation

$$\xi^2 f_{\xi\xi} + \xi f_\xi + (\xi^2 - 1)f = 0 \tag{3.5}$$

with bounded solution

$$f(\xi) = AJ_1(\xi) \tag{3.6}$$

where A is, as yet, an undetermined constant and $J_1(\xi)$ is the Bessel function of the first kind. The radial velocity $u(r, \theta, t)$ computed from (3.1a) permits the evaluation of boundary condition (3.3) yielding

$$A = \frac{C_0 X_0 \omega}{g J_1'(\omega R/C_0)}. \tag{3.7}$$

The equation (2.7) for the motion of the container

$$m_0 \ddot{X} + (m + m_0)\omega_0^2 X = F_p \tag{3.8}$$

necessitates evaluation of the net sideways hydrostatic pressure force acting on the cylindrical wall with outward normal $\mathbf{n}$

$$F_p = \int p(\mathbf{n} \cdot \mathbf{i}) dS = \rho g \pi A R H J_1(\omega R/C_0) \cos \omega t \tag{3.9}$$

in which it may be seen that the steady contribution to the integral is identically zero. In (3.9) the surface integral is over the wetted surface of the cylinder, which for the linear theory is $z \in [-H, 0]$ and $\theta \in [0, 2\pi]$. Inserting the result for F_p into (3.8) and dividing by the container mass m_0 yields

$$\ddot{X} + \Omega^2 X = \frac{gAM}{R} J_1(\omega R/C_0) \cos \omega t \tag{3.10}$$

where again M is the fluid/container mass ratio and Ω is the previously defined fluid-augmented pendulum frequency (2.10) with $n = 1$ in this case. Compatibility of (3.10) with the assumption $X(t) = X_0 \cos \omega t$ furnishes, with the aid of equation (3.7), the eigenvalue relation

$$RJ_1'(\omega R/C_0)(\omega^2 - \Omega^2) + MC_0\omega J_1(\omega R/C_0) = 0 \tag{3.11a}$$

which can be shown to agree with equation (35) of Yu (2010). For the fundamental seiche mode, the extreme amplitudes of fluid motion occur at $r = R$ when $\theta = 0, \pi$; hence the amplification factor for this mode is given by

$$\frac{\eta_0}{X_0} = \left(\frac{C_0\omega}{g}\right) \frac{J_1(\omega R/C_0)}{J_1'(\omega R/C_0)}. \tag{3.11b}$$

Analogous to the parameter μ for the box problem we have the parameter $\nu = lm_0/\pi\rho R^4$. The dimensionless forms of equations (3.11) are then

$$\left(\frac{\omega}{\omega_0}\right)^2 = (1 + M) - \nu^{1/2} M^{3/2} \left(\frac{\omega}{\omega_0}\right) \frac{J_1\left(\dfrac{\omega/\omega_0}{\sqrt{\nu M}}\right)}{J_1'\left(\dfrac{\omega/\omega_0}{\sqrt{\nu M}}\right)} \tag{3.12a}$$

and

$$\frac{\eta_0}{X_0} = \frac{R}{l}\left(\frac{\omega}{\omega_0}\right)(\nu M)^{1/2} \frac{J_1\left(\dfrac{\omega/\omega_0}{\sqrt{\nu M}}\right)}{J_1'\left(\dfrac{\omega/\omega_0}{\sqrt{\nu M}}\right)}. \tag{3.12b}$$

For the fundamental mode of synchronous sloshing $0 \leq \omega/\omega_0\sqrt{\nu M} \leq j_{1,1}'$ where $j_{1,1}' = 1.84118$ is the first zero of $J_1'(\xi)$.

As an example, we present the lowest in-phase mode frequencies calculated from Eq. (3.12a) for a cylindrical container in figure 5 calculated for different values of ν.

4 Wedge geometry

Recall that Cooker (1994) used potential theory, assuming hydrostatic pressure, to find a solution for a suspended planar hyperbolic container. The asymptotes of these hyperbolae form a wedge with apex angle 90°. The streamlines for this geometry coincide with those depicted by Lamb (1932, §258). For this limiting geometry, Cooker (1994) presented a formula for the frequency of suspended container motion that exhibits two frequencies, the lower (higher) of which corresponds to wave oscillations in phase (anti-phase) with the motion of the oscillating wedge given by

$$\left(\frac{\omega}{\omega_0}\right)^2 = \frac{(1+M)}{2k}\left[(1+k) \pm \sqrt{(1+k)^2 - \frac{4k}{(1+M)}}\,\right] \tag{4.1}$$

where $k = H/l$. This is exactly Cooker's result, now using M *in lieu* of R, so that one must remember that the quiescent fluid depth H is dependent on M through the relation $H = \sqrt{m_0 M/\rho W}$.

Experiments to be presented in §5.3 show that this result consistently over-predicts the experimental measurements for all values of M. Communication with Cooker led to a correction of the theory for this case, wherein application of the hydrostatic pressure at the sidewalls is replaced by the potential pressure. The revised theory (personal communication with M. J. Cooker, 2009) is that given by linearized potential theory. In hindsight, it is clear that all solutions for the motion of the suspended wedge with 90° apex angle must be governed by just one formulation because the streamlines for each liquid volume placed in the wedge are self-similar: thus finite-depth potential theory is the only possibility.

The governing linearized boundary-value problem for potential flow in a frame of reference moving with the container are given as

$$\nabla^2\phi = 0 \tag{4.2a}$$

in the fluid domain to be solved with the linearized kinematic and dynamic free-surface conditions

$$\phi_z = \eta_t, \qquad \phi_t + g\eta + x\ddot{X} = 0 \qquad (z = 0) \tag{4.2b}$$

with impermeability on the wedge side-walls

$$\mathbf{n}\cdot\boldsymbol{\nabla}\phi = 0, \qquad z = -h(x) \tag{4.2c}$$

where for a 90° wedge

$$h(x) = H + x \quad (-H \le x \le 0); \qquad h(x) = H - x \quad (0 \le x \le H). \tag{4.2d}$$

Combining the kinematic and dynamic free-surface conditions furnishes the equation

$$\phi_{tt} + g\phi_z + x\ddot{X} = 0 \qquad\qquad (z = 0). \tag{4.3}$$

Positing the solution

$$\eta(x,t) = \eta_0 \frac{x}{H} \cos\omega t \tag{4.4a}$$

and solving the above boundary-value problem for the potential function using the periodic sideways displacement $X = X_0 \cos\omega t$ yields

$$\phi(x,z,t) = x\left[X_0\omega - \left(\frac{g\,\eta_0}{\omega\,H}\right) - \left(\frac{\omega\,\eta_0}{H}\right)\,z\right]\sin\omega t. \tag{4.4b}$$

Now applying the impermeability condition (4.2c) furnishes the relation for the inverse amplification ratio

$$\frac{\eta_0}{X_0} = \left(\frac{g}{h\,\omega^2} - 1\right)^{-1}. \tag{4.5}$$

The linearized form of Bernoulli's equation

$$p = -\rho\left[\phi_t + gz + x\ddot{X}\right] \tag{4.6}$$

is now used to compute the pressure given as

$$p(x,z,t) = \rho\left[x\left(\frac{g\eta_0}{H} + \frac{\eta_0\omega^2}{H}\,z\right)\cos\omega t - gz\right]. \tag{4.7}$$

Integrating the horizontal component of the pressure over the internal surface of the wedge furnishes the pressure force

$$F_p = \int p(\mathbf{n}\cdot\mathbf{i})dS = \rho\left(gH - \frac{1}{3}\omega^2H^2\right)\eta_0\,\cos\omega t \tag{4.8}$$

and the pendulum restoring force is

$$F_r = -(m_0 + m)\frac{g}{l}X. \tag{4.9}$$

Inserting these forces into the governing equation of motion

$$m_0\ddot{X} = F_r + F_p \tag{4.10}$$

gives a second relation for the inverse amplification ratio, *viz.*

$$\frac{\eta_0}{X_0} = \left(\frac{\frac{1}{3}\omega^2 - \dfrac{g}{H}}{\omega^2 - (1+M)\dfrac{g}{l}}\right)^{-1}. \tag{4.11}$$

Equating the results in (4.5) and (4.11) gives a quartic equation for the oscillation frequency ω, the solution of which is

$$\left(\frac{\omega}{\omega_0}\right)^2 = C\left(\frac{1+k}{2k}\right)\left[1 \pm \sqrt{1 - \frac{4k}{C(1+k)^2}}\right] \tag{4.12a}$$

in which

$$C = \frac{1+M}{1+\dfrac{M}{3}}, \qquad k = \frac{H}{l}. \tag{4.12b}$$

The plus/minus signs correspond to anti-phase/in-phase fluid oscillations, respectively, and these are the only modes obtained for this particular geometry for which the liquid surface always remains flat: *cf.* Eq. (4.4a). Another distinction between the wedge geometry and the box and cylinder geometries is that the in-phase wedge frequencies tend to the correct dry container frequency ω_0 as $M \to 0$.

The deep-water frequencies computed here are compared with the shallow-water results of Cooker (1994) for in-phase sloshing in a wedge container of width $W = 0.5$ m, mass $m_0 = 4.0$ kg, liquid density $\rho = 1000$ kg/m^3, in the gravitational field $g = 9.80$ m/s^2 suspended on pendulum wires of length $l = 0.5$ m in figure 6a; corresponding results for the anti-phase oscillations are displayed in figure 6b. Note that the in-phase motion frequencies obtained from potential theory are significantly higher than those obtained using the shallow-water theory and calculations show that this disparity increases with decreasing pendulum length l. The disparity in frequencies for the anti-phase oscillations is even more dramatic at large M where figure 6b shows a slowly decreasing frequency for the potential theory and a rapidly increasing frequency for the shallow-water result. Both anti-phase results exhibit blow-up as $M \to 0$. These anti-phase solutions are the only possible modes for sloshing in free containers and the tendency for the frequencies to grow with decreasing liquid mass has been documented in the free container experiments of Herczynski and Weidman (2012).

5 Experiments

Experiments were conducted for the bifilar pendulum motion of a two-chamber box, a three-chamber box, a cylinder and a 90° wedge. The experiments were constructed and performed in the following manner. A heavy aluminum plate was mounted and leveled across the rafters of the garage of PDW. The bifilar suspension system was constructed using three equal length 1/16-inch steel wire ropes with compression eyelet sleeves. Opposite ends of the eyelets were

inserted into assemblies designed to house two SR3-ZZEEC Boca bearings separated to accommodate the eyelets using a shoulder bolt; a detailed sketch of the bearing assemblies may be found in Weidman *et al.* (2015). One wire was located at the center front of a container and the two other wires were symmetrically disposed aft of the container. Five three-wire sets were made to nominal eyelet hole to eyelet hole lengths $l = \{0.5, 1.0, 1.5, 2.0, 2.5\}$ m. The measured average lengths are listed in Table 1. Note that in experiments the two parameters convenient to vary are the pendulum length l and the fluid mass m. Therefore because the rectangular container parameters $m_0,\ D_n,\ W_n$ and fluid density ρ are fixed, then μ_n from (2.20) and M_n from (2.8) are the corresponding non-dimensional parameters to l and m respectively. Likewise, the corresponding non-dimensional parameters for the cylinder are ν and M and l/H and M for the 90° wedge.

Wire Set	Nominal l (m)	Measured l (m)
l_1	0.5	0.49889
l_2	1.0	1.0018
l_3	1.5	1.5034
l_4	2.0	2.0019
l_5	2.5	2.5016

Table 1. Nominal and measured average wire rope lengths l used in the experiments.

All containers were fabricated using clear plexiglass. The two-chamber and three-chamber boxes were constructed using 1/8-inch material and affixed with brackets at the upper sides on which the lower bearing assemblies were mounted. Directly above, the upper bearing assemblies were attached to the heavy aluminum plate. The boxes had horizontal top plates above each chamber, so water was introduced and extracted through small semicircular openings made in the upper center faces on opposite sides of each chamber. The circular cylinder and the base plate to which it was glued were made of 1/4-inch plexiglass; in this case the bearings were mounted to the top of the base plate. The 90° wedge was also fabricated using 1/4-in plexiglass and was suspended from bearing assemblies mounted on narrow horizontal plexiglass strips glued to the top on opposite ends of the wedge.

The internal dimensions of the box chambers, cylinder and wedge where fluid could be introduced are given in Table 2. Observe that the boxes and wedge were suspended from the top while the cylinder was suspended from the bottom. Owing to the heights of the containers and the points of suspension, the maximum wire rope lengths that could be

accommodated in the garage for the two-chamber box and wedge was 2.0 m, that for the three-chamber box was 1.5 m, whilst that for the cylinder was 2.5 m.

Container	Length (m)	Height (m)	Width (m)	Weight (kg)
Two-chamber Box	0.4997	0.4191	0.3485	5.5793
Three-chamber Box	0.4988	0.6223	0.3461	7.8205
Cylinder	0.4413	0.2127	—	5.8760
Wedge	0.6097	0.3049	0.3536	5.7448

Table 2. Internal lengths L (or diameter in the case of the cylinder), heights H, widths W of the box chambers, cylinder and 90° wedge. Also shown are the container weights supported by the pendula wires. The container weights include the necessary brackets and bearing assemblies to which the pendulum wires are attached.

The protocol for experimentation was to successively add equal volumes of water to a container, pull it back from its vertical equilibrium position on the order of 10-20 cm using a strong piece of thread, and burn the thread with a cigarette lighter to allow the container to begin its motion with zero impulse. Initial disturbances were as observed by Cooker (1994) but the system ultimately settled down to simple periodic motion with in-phase sloshing of the liquid. Owing to viscous friction, the oscillation amplitude decayed over time, but sufficient time was available for a stopwatch measurement of the period averaged over ten oscillations.

We now present experimental measurements of the oscillation frequency of the containers which are compared with the theoretical results for each geometry tested.

5.1 Multi-chamber boxes

The first order of business was to affirm the empty container oscillation frequency. We measured this frequency for the two-chamber and three-chamber boxes, the cylinder and the 90° wedge. These results are presented in figure 7.

We also wanted to demonstrate that it does not matter which compartment of a multi-box container is filled to obtain the frequency of motion in bifilar suspension. This is verified in figure 8 wherein oscillation frequencies were measured in the two-chamber box using fillings in either the lower or upper chamber for a pendulum length $l = 1.5$ m.

Next we measured the oscillation frequencies in the two-chamber box as a function of added fluid mass for pendulum lengths $l = \{0.5, 1.0, 1.5, 2.0\}$ m using fillings in the upper

chamber only. These results presented in figure 9 show excellent agreement with shallow-water theory.

Then we added equal volumes of water to each chamber in the two-chamber box and measured the oscillation frequencies. These results presented in figure 10 for pendulum lengths $l = \{0.5, 1.0, 1.5, 2.0\}$ m also show excellent agreement with shallow-water theory.

Finally, we present results for equal volume fillings in each chamber of the three-chamber box. These frequencies displayed in figure 11 for pendulum lengths $l = \{0.5, 1.0, 1.5\}$ m again show excellent agreement with shallow-water theory.

5.2 Cylinder

Although the theory for a multi-cylindrical container (possibly with variable diameters) is possible, we here present measurements for a single cylinder under bifilar suspension. Because the cylinder was supported at its base plate, we were able to conduct experiments for all wire rope lengths $l = \{0.5, 1.0, 1.5, 2.0, 2.5\}$ m. The results of these experiments are shown in figure 12 where again good agreement with shallow-water theory is observed.

5.3 Wedge

For the available pendulum lengths, measurement of the frequencies observed by releasing the wedge from a displaced position at zero velocity gives only in-phase oscillations of the fluid with respect to the container. Experimental results for pendulum lengths $l = \{0.5, 1.0, 1.5, 2.0\}$ m are displayed in figure 13. Note the expanded scale of the ordinate in this figure compared to the frequency scales given for the boxes and cylinders. There is clearly excellent agreement between potential theory and experiment, even for $l = 0.5$ m where the experimental data lie continuously above the theory; we note that the maximum discrepancy observed at $m/m_0 \doteq 3$ is less than 0.9%.

The small deviations of the theoretical and experimentally measured frequencies for the wedge at $l = 0.5$ m are likely to be due to the additional system mode being significant in the solution and modulating the container motion. The result in figure 15a (see §6) shows this is the case for the rectangular container; the same observation is expected when the additional asynchronous mode appears for the wedge at small pendulum lengths.

6 Theory for small fluid to container mass ratios

With the possible exception of the 90° wedge, the above experimental results all show excellent agreement with the shallow-water theory derived in §§2-4. However the single chamber results for $l = 0.5$ m demonstrate an interesting behavior for $m/m_0 \lesssim 0.5$. Here the oscillation frequency of the system appears to 'jump' to a higher frequency eigensolution. These experimental results are shown in figure 14, with the corresponding higher frequency roots of the single-compartment version of (2.11), namely

$$\left(\frac{\omega}{\omega_0}\right)^2 = 1 + M_1 - \mu_1^{1/2} M_1^{3/2} \left(\frac{\omega}{\omega_0}\right) \tan\left(\frac{\omega/\omega_0}{\sqrt{\mu_1 M_1}}\right). \tag{6.1}$$

The fundamental seiche mode is given by $i = 1$, and we denote $i = 2$ the second anti-symmetric sloshing mode, $i = 3$ the third anti-symmetric sloshing mode, etc. The roots of Eq. (6.1), ω_i for $i = 1,\ 2,\ 3, ...$, were found via a root finding algorithm for nonlinear equations, such as Newton iteration. The results in figure 14 show that the frequency of the box is in good agreement with the second anti-symmetric sloshing mode for the two experimental points found.

The reason this mode switching occurs is due to the initial condition of the experimental system where $X(0) = 0.1$ m and $\eta(x, 0) = 0$. This initial condition sets up a solution which contains a superposition of the anti-symmetric sloshing eigenmodes, i.e. the box displacement is of the form

$$X(t) = \sum_{i=1}^{\infty} X_i \cos(\omega_i t), \tag{6.2}$$

where the X_is are constants determined by the initial condition. This container displacement is contrary to that in (2.2) which assumes only a single frequency solution, i.e. that $X_i = X_0$ for some i and $X_i = 0$ for all other modes. The time evolution of the box displacement, using the same initial condition as the experiments, can be simulated using the linear shallow-water numerical scheme in §8.1 of Alemi Ardakani & Bridges (2010). This scheme uses a Lagrangian Particle Path formulation to simulate the shallow-water equations, and the reader is directed to this paper for complete details of the scheme, including the numerical formulation. The simulation of $X(t)$ for $m/m_0 = 2.5,\ 1.0$ and 0.5 are given by the solid lines in figure 15. The dashed line in figures 15a-15c give the corresponding linear result for the fundamental ($i = 1$) mode only and the dashed line in figure 15d gives the result for the second anti-symmetric mode ($i = 2$) only. These simulations show that at $m/m_0 = 2.5$, despite having some superposed higher frequency oscillations, the box displacement approximately agrees with

the fundamental frequency solution. As the mass ratio decreases the magnitude of the second anti-symmetric mode increases until at $m/m_0 = 0.5$ the frequency of the box displacement $X(t)$ is in good agreement with this mode. Thus the apparent 'jumping' between eigenmodes seen in figure 14, is in fact a *smooth transition* between modes, but experimental verification of a single frequency in this transition region would be difficult.

As we are in the linear amplitude regime, the modes in the solution (6.2) do not interact with each other, hence we can calculate which mode dominates the solution by determining the values for the constants X_i from (6.2) as a function of m/m_0. We determine these constants by ensuring the initial conditions are satisfied, namely that

$$X(0) = 0.1 \text{ m} = \sum_{i=1}^{\infty} X_i, \tag{6.3a}$$

and

$$\eta(x,0) = 0 = \sum_{i=1}^{\infty} X_i \frac{H_1 \omega_i \tau_1}{D_1 \cos(\omega_i \tau_1)} \sin[\omega_i \tau_1 (x/D_1)] \qquad \text{for} \qquad -D_1 \leq x \leq D_1. \tag{6.3b}$$

We satisfy the free-surface condition (6.3b) at the $N-1$ points $x_j = (j-1)/(N-1)D_1$ for $j = 1, ..., N-1$, which together with (6.3a), leads to a system of N linear equations

$$\mathbf{A}\mathbf{x} = \mathbf{b}, \tag{6.4}$$

where

$$\mathbf{A} = \begin{bmatrix} 1 & 1 & \cdots & 1 \\ \frac{H_1\omega_1\tau_1 \sin[\omega_1\tau_1(x_1/D_1)]}{D_1\cos(\omega_1\tau_1)} & \frac{H_1\omega_2\tau_1 \sin[\omega_2\tau_1(x_1/D_1)]}{D_1\cos(\omega_2\tau_1)} & \cdots & \frac{H_1\omega_N\tau_1 \sin[\omega_N\tau_1(x_1/D_1)]}{D_1\cos(\omega_N\tau_1)} \\ \vdots & \vdots & \ddots & \vdots \\ \frac{H_1\omega_1\tau_1 \sin[\omega_1\tau_1(x_{N-1}/D_1)]}{D_1\cos(\omega_1\tau_1)} & \frac{H_1\omega_2\tau_1 \sin[\omega_2\tau_1(x_{N-1}/D_1)]}{D_1\cos(\omega_2\tau_1)} & \cdots & \frac{H_1\omega_N\tau_1 \sin[\omega_N\tau_1(x_{N-1}/D_1)]}{D_1\cos(\omega_N\tau_1)} \end{bmatrix}, \tag{6.5a}$$

and

$$\mathbf{x} = (X_1, X_2, ..., X_N)^T, \qquad \mathbf{b} = (0.1, 0, ..., 0)^T. \tag{6.5b}$$

We find that using $N = 20$ leads to converged values for the first eight coefficients of $\mathbf{x}$, and X_1 to X_4 are presented as a function of m/m_0 in figure 16. These results nicely explain the results of the simulations in figure 15. For $m/m_0 = 2.5$ the fundamental mode dominates the solution, but with quite a large contribution from the 2nd anti-symmetric mode. The 2nd anti-symmetric mode begins to dominate the motion of the box around $m/m_0 = 1.5$ and by $m/m_0 = 0.5$ it is the dominate mode, as demonstrated in figure 15d. Figure 16 also shows

that as the mass ratio is reduced further, each anti-symmetric mode dominates the solution in turn, albeit for a successively smaller range of fluid heights. The value of m/m_0 where the maximum values of X_i occur for $i = 1, ..., 6$ are given in table 3. Thus the result in figure 16 shows that $\omega \to \omega_0$ as $m/m_0 \to 0$, as expected. It should be noted here that measuring the frequency of the experimental system in these regions is very difficult due to the occurrence of higher and lower frequency modes in the solution modulating the container motion $X(t)$, hence the limited number of experimental data points obtained.

Anti-symmetric mode number	Rectangular box	Cylinder
$i = 1$	∞	∞
$i = 2$	0.3882	0.1718
$i = 3$	0.1002	0.0519
$i = 4$	0.0443	0.0246
$i = 5$	0.0248	0.0143
$i = 6$	0.0159	0.0094

Table 3. Values of m/m_0 where the maximum value of X_i occurs for the first 6 anti-symmetric modes for both the single rectangular box and the cylinder with $l = 0.5$ m in each case.

The same phenomena was also observed for the cylindrical container, see figure 17, but in this case only one experimental point was observed with the higher oscillation frequency. The reason for this can be seen in the values of the mode coefficients X_i in figure 18 and the position of their maximums in table 3. These results were obtained in a similar manner as for the rectangular container results, except with $\eta(x, t)$ given by (3.4) with $\theta = 0$. Here the position of the maximum values of X_i occur for smaller values of m/m_0 than for the rectangular box, and hence only the single measured point is seen to agree with the second eigenvalue of (3.12a). These results also show that ω does in fact tend to ω_0 as $m/m_0 \to 0$, as expected, for the cylindrical container.

7 Discussion and Conclusion

The governing equations for a single suspended fluid-filled box of uniform rectangular section reveals that the dimensionless frequency ω/ω_0, wavelength $\lambda/2D$, and amplification ratio η_0/X_0 are fully described by just three independent dimensionless parameters: M, μ and X_0/D. Dimensional analysis shows that the system is potentially dependent on two

additional length ratios W/D and l/D, but the shallow-water theoretical analysis shows that these parameters have already incorporated into the system and thus do not appear explicitly.

The general eigenvalue relation describing the frequency of synchronous motion for suspended multi-compartment containers derived by Turner *et al.* (2013) has been re-derived in terms of the independent dimensionless parameters above. Solutions show that the distribution of a given quantity of fluid uniformly across identical multiple compartments reduces the fundamental (in-phase) frequency ω_1 of synchronous motion with increasing number of compartments. Furthermore, the fundamental frequencies satisfy $0 < \omega/\omega_0 < 1$ and the limit as $M \to 0$ is nonuniform. Disturbance wavelengths all emanate from the dry container limit $\lambda/L = 2$ and increase without bound with increasing fluid mass.

The suspended motion of rectangular containers of differing horizontal lengths (*cf.* figure 3) filled to the same total volume of equal density liquid were analyzed with results shown in figure 4. One finds that the 'single' box exhibits the lowest frequency and that the frequencies increase as one proceeds to the 'boxes', the 'triple', and the '3deep' configurations.

A linearized shallow-water analysis has been made of synchronous sloshing in a bifialar suspended cylindrical container. Results qualitatively similar to those obtained for rectangular boxes are found. In both geometries the lowest mode for free and suspended motion may be described by fluid sloshing about a central nodal line oriented normal to the direction of sideways movement of the container.

The 90° wedge experiments are in accord with theory only when potential theory is employed. It is to be noted that the out-of-phase modes for the wedge were not accessible in the present set of experiments as our shortest pendulum wire length $l = 0.5$ m was not sufficiently short to observe these modes. In a new study by the authors (Turner & Weidman, 2016) these out-of-phase modes are shown to appear in hyperbolic containers at short pendulum lengths. As a result, a future experimental study is envisioned to document the out-of-phase sloshing modes for both the 90° wedge and the hyperbolic container.

Experimental results for the single chamber box and the cylinder with a pendulum length $l = 0.5$ m showed that the frequency of the container motion transitioned from that of the lowest frequency fundamental mode to the second lowest frequency mode as the mass ratio m/m_0 was reduced. This can be theoretically explained by considering a solution comprising of an infinite sum of all frequency modes and determining their pre-factor coefficients such that the container displacement and free-surface elevation satisfy the experimental initial conditions. These results show that as the fluid/container mass ratio is reduced, the solution

is dominated by successively higher frequency modes such that the container frequency $\omega \to \omega_0$ as $m/m_0 \to 0$, as expected. Therefore, even though the results here are independent of the magnitude of the dominant mode, because the system is linear, they show that the ratio of the mode magnitudes, e.g. $|X_1|/|X_2|$, are significant to the overall solution, especially as $M \to 0$.

Cooker's (1994) paper has stimulated renewed interest in the dynamical interaction between a fluid and its container. The low-amplitude suspended pendulum problem is relatively straightforward because the container is confined to move horizontally in time. With this constraint removed, fluid-container interaction problems become more complicated especially when nonlinear effects are included.

ACKNOWLEDGEMENTS

The authors gratefully acknowledge informative discussions with Dr. M. J. Cooker, Professor Francisco Higuera, Dr. H. Alemi Ardakani and Professor T. J. Bridges on the subject of this paper. Special thanks are accorded Peggy Bunch who assisted in many of the experiments.

References

Alemi Ardakani, H. and Bridges, T. J. 2010 Dynamic coupling between shallow-water sloshing and horizontal vehicle motion, Euro. J. Appl. Math., 21, 479-517.

Alemi Ardakani, H., Bridges, T. J. and Turner, M. R. 2012 Resonance in a model for Cooker's sloshing experiment, Euro. J. Mech. B/Fluids, 36, 25-38.

Abramson, H. N. 1966 The dynamical behavior of liquids in a moving container. Tech. Rep. SP-106, NASA, Washington, DC.

Cooker, M. J. 1994 Water waves in a suspended container. Wave Motion, 20, 385-395.

Cooker, M. J. 2009 Personal communication.

Herczynski, A. and Weidman, P. 2012 Experiments on the periodic oscillations of free containers driven by liquid sloshing, J. Fluid Mech., 693, 216-242.

Lamb, H. 1945 Hydrodynamics, 6th Edition, Cambridge University Press, Dover Publications, New York.

Linton, C. M. and McIver, P. 2001 Handbook of Mathematical Techniques for Wave-Structure Interaction, Chapman & Hall/CRC, Boca Raton.

Moiseev, N. N. 1964 Introduction to the theory of oscillations of liquid-containing bodies. Adv. Appl. Mech., 8, 233-289.

Murphy, G. 1950 Similitude in Engineering, The Ronald Press Co., New York.

Stoker, J.J. 1957 Water waves: the mathematical theory with applications. Interscience Publishers, New York.

Turner, M. R., Bridges, T. J. and Alemi Ardakani, H. 2013 Dynamic coupling in Cooker's sloshing experiment with baffles, Phys. Fluids, 25(10), 112102.

Turner, M. R. and Weidman, P. D. Coupled sloshing in hyperbolic containers suspended as a bifilar pendulum, submitted to *Physical Review Fluids*.

Weidman, P. D., Herczynski, A., Yu, J. and Howard, L. 2015 Experiments on standing waves in a rectangular tank with corrugated bed, J. Fluid Mech., 777, 122-150.

Yu, J. 2010 Effects of finite water depth on natural frequencies of suspended water tanks, Stud. Appl. Math., 125, 337-391.

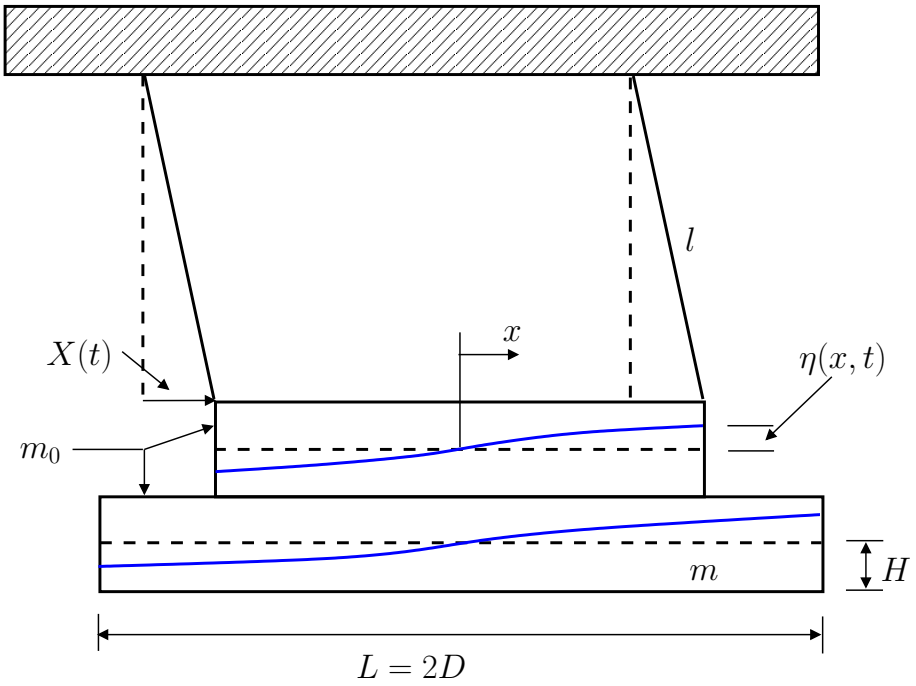

Figure 1. Sketch of a fluid-filled multicompartment container suspended as a bifilar pendulum. The free surface displacement of the liquid is $\eta(x,t)$ relative to the horizontal displacement $X(t)$ of the container. Each n^{th} chamber has its own width W_n, length L_n, liquid depth H_n, liquid density ρ_n, and free surface waveform η_n.

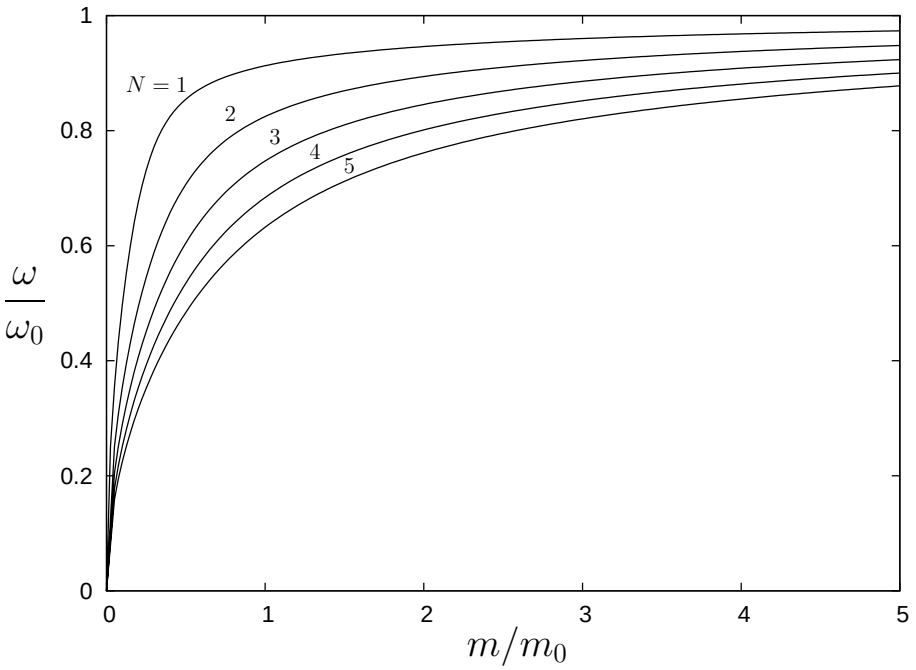

Figure 2. Theoretical normalized oscillation frequencies as a function of mass ratio m/m_0 for a box composed of five identical chambers filled by the scenario

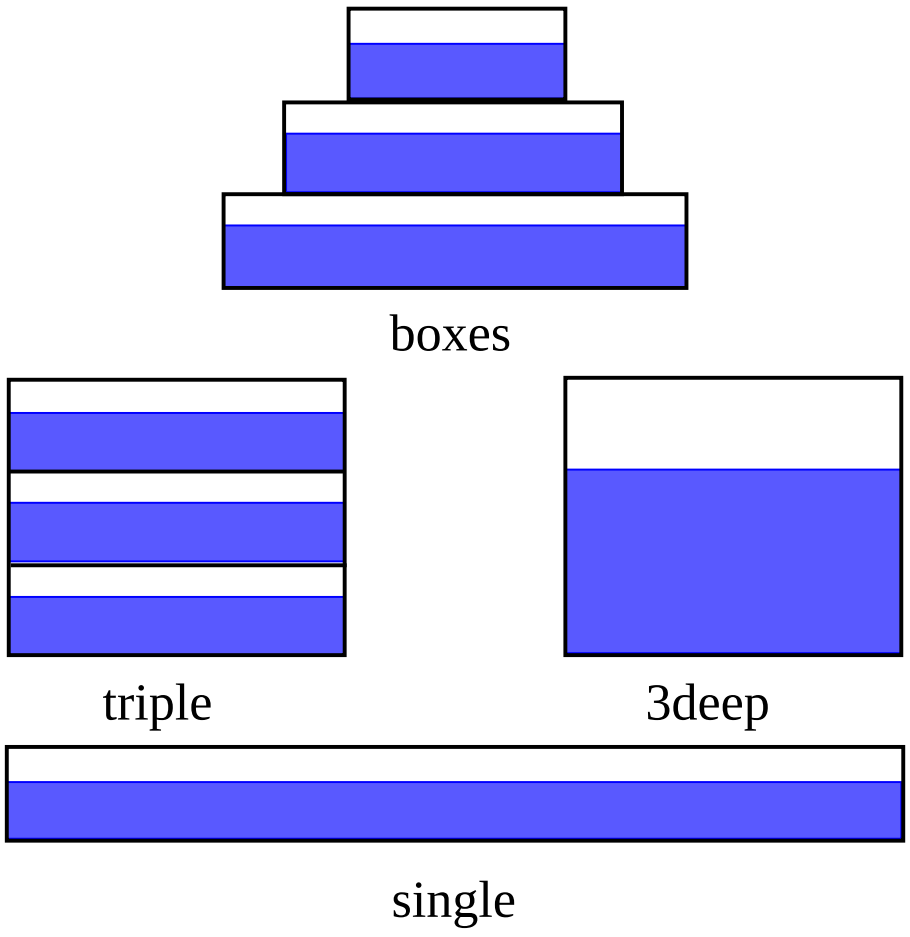

Figure 3. Sketch of four containers each filled with the same fluid mass. The configurations are referred to as (a) 'boxes', (b) 'triple', (c) '3deep', and (d) 'single' configurations. All widths are $W = 0.1$ m and the horizontal dimension for the chambers are (a) $L_1 = 0.8$ m, $L_2 = 0.6$ m, and $L_3 = 0.4$ m, (b) $L_1 = 0.6$ m, (c) $L_1 = 0.6$ m and (d) $L_1 = 1.8$ m, and the assumed common container mass is $m_0 = 1.0$ kg.

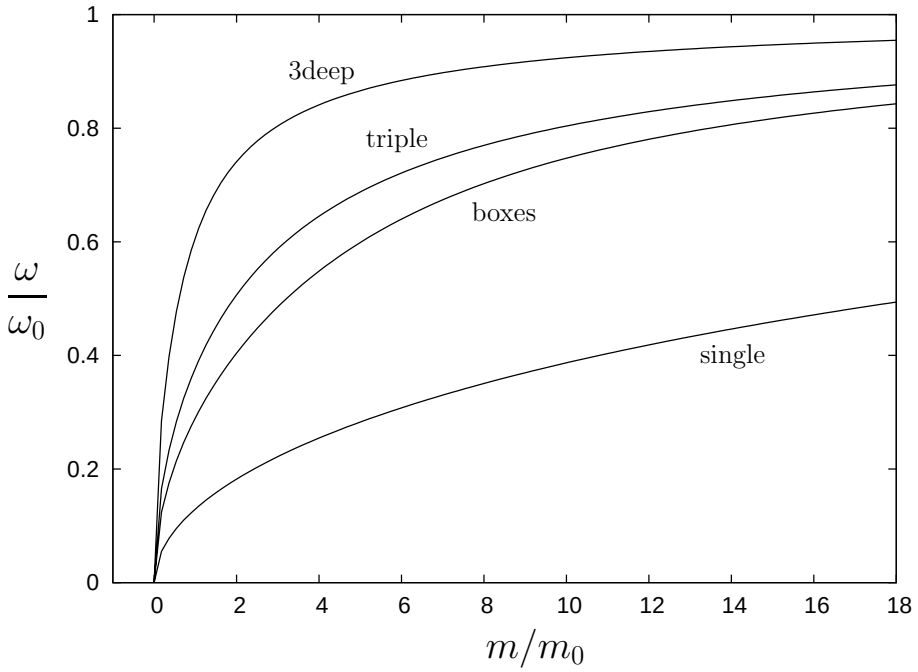

Figure 4a. Dimensionless frequency as a function of dimensionless fluid mass for the continuous filling of the suspended 'boxes', 'triple', '3deep', and 'single' configurations sketched in figure 3. The selected pendulum length is $l = 1.0$ m giving the reference frequency $\omega_0 = 3.130$ rad/sec.

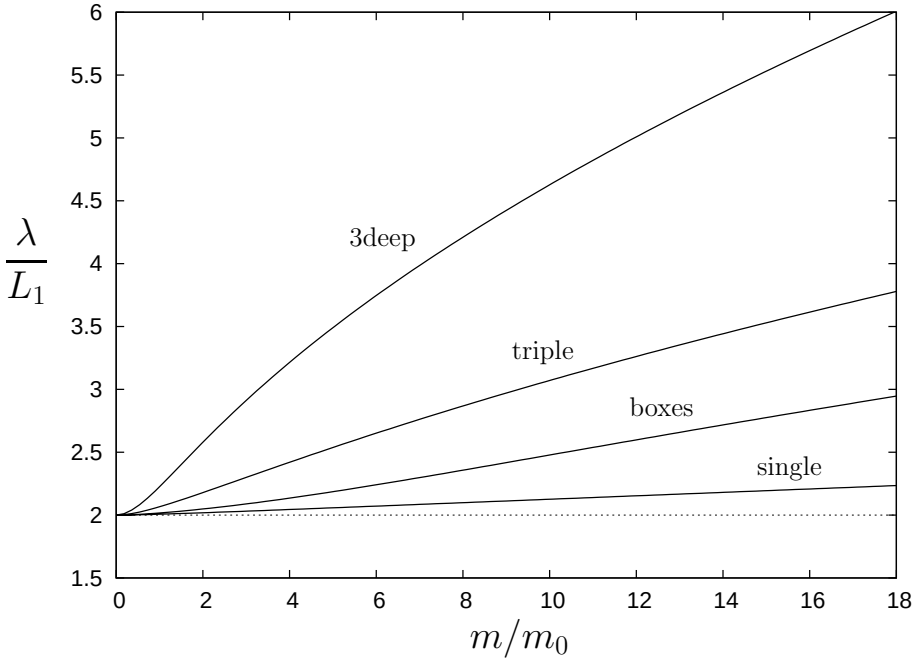

Figure 4b. Dimensionless wavelength as a function of dimensionless fluid mass for the continuous filling of the suspended 'boxes', 'triple', '3deep', and 'single' configurations. The reference lengths L_1 are given in the caption of Figure 3.

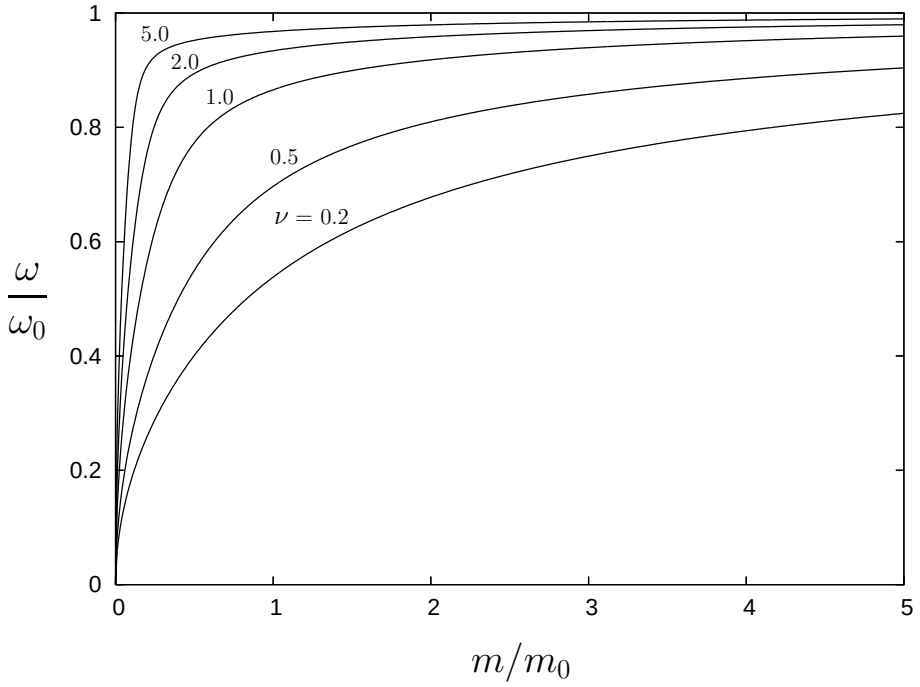

Figure 5. Normalized oscillation frequencies as a function of dimensionless fluid mass at selected values of ν for synchronous in-phase sloshing in a suspended cylindrical container.

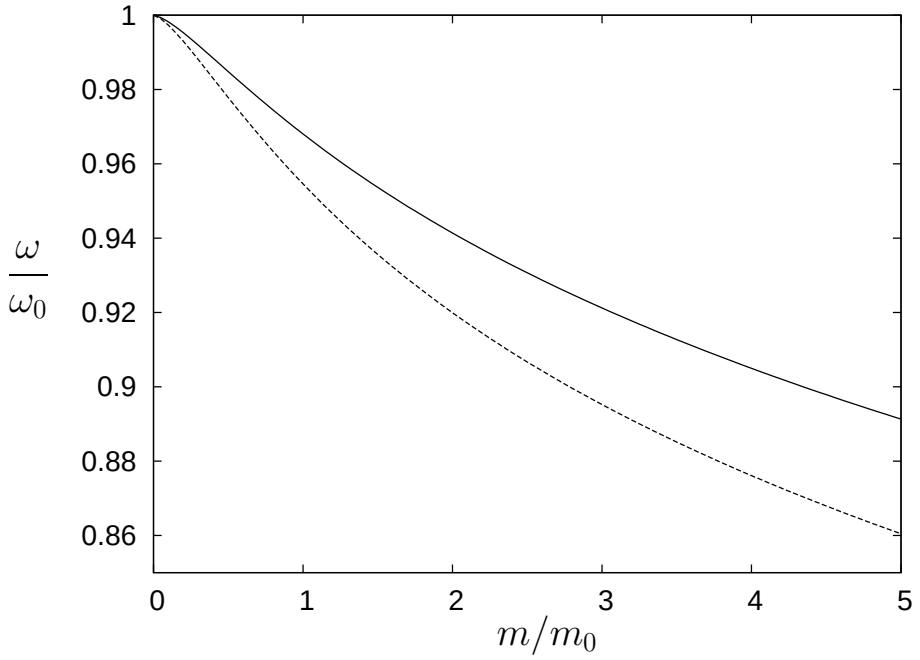

Figure 6a. Comparison of in-phase frequencies in a 90° wedge based on the formula of Cooker (1994) (dashed line) and the potential theory result (solid line).

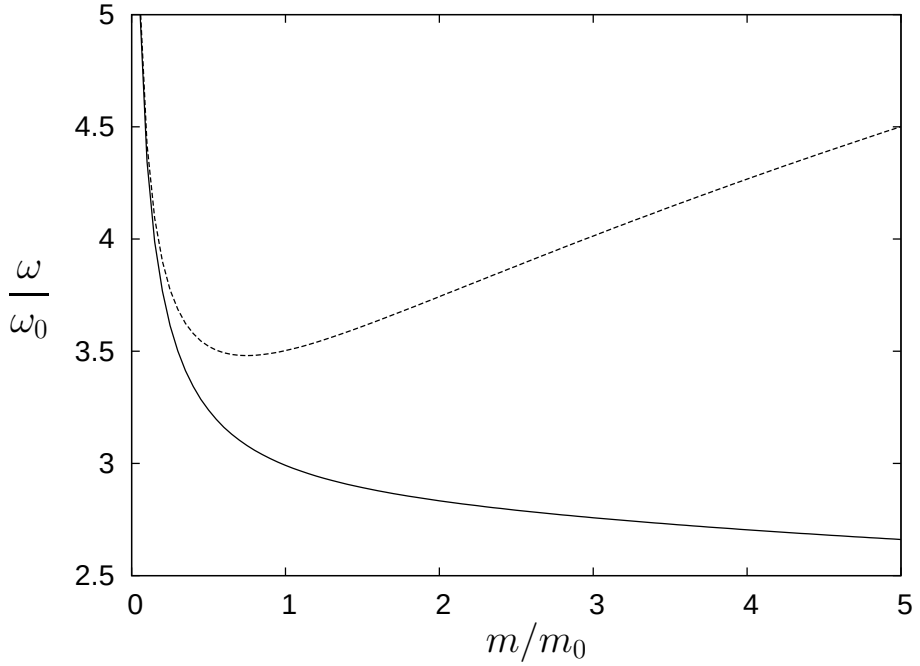

Figure 6b. Comparison of out-of-phase frequencies in a 90° wedge based on the formula of Cooker (1994) (dashed line) and the potential theory result (solid line).

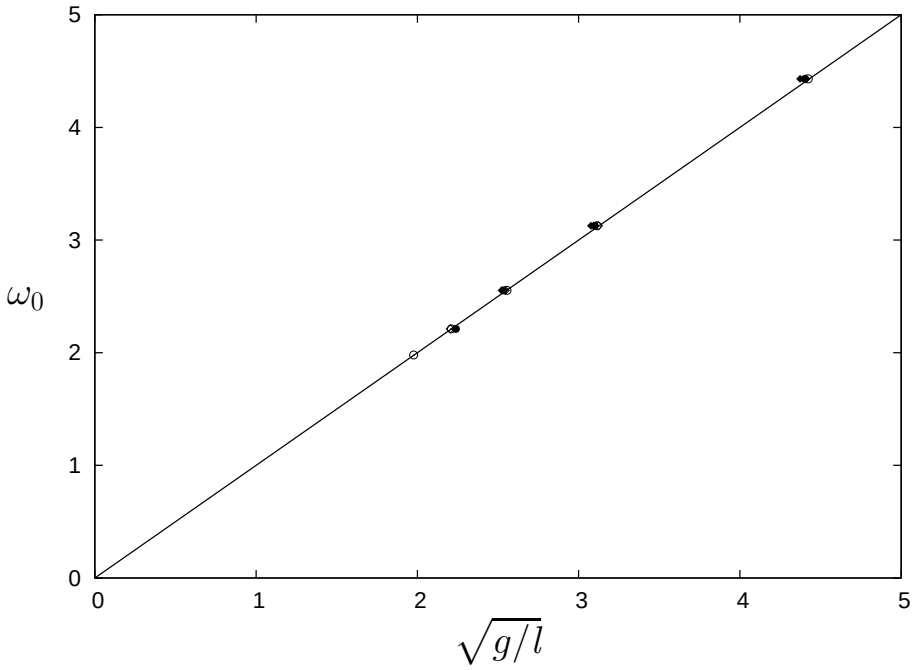

Figure 7. Measured empty container pendulum oscillation frequencies for the two-chamber box (solid circles), cylinder (open circles), 90° wedge (solid diamonds) and the three-chamber box (open diamonds) for pendulum lengths used in the experiment.

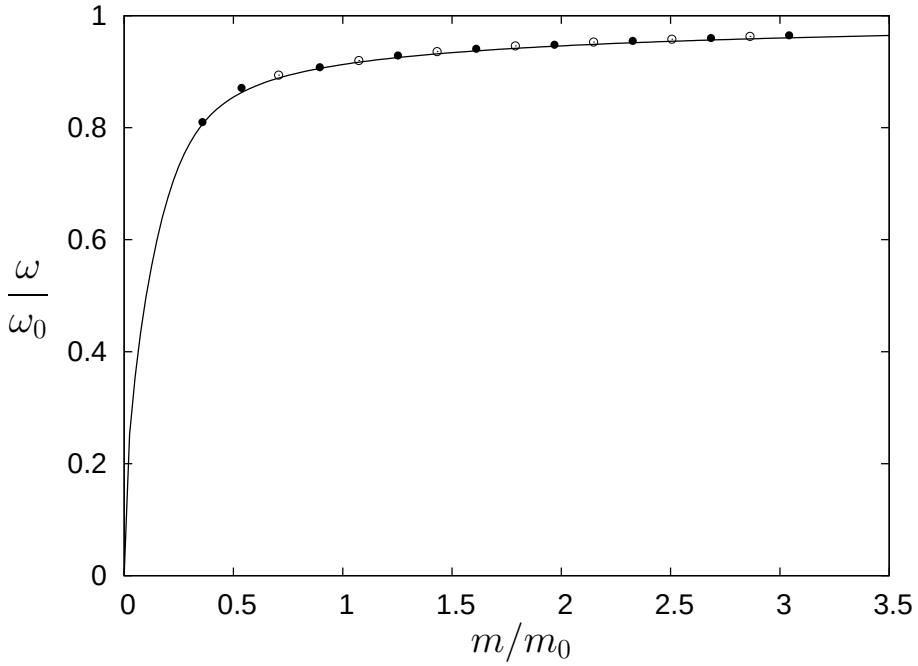

Figure 8. Measured oscillation frequencies for the two-chamber box using either upper chamber (solid circles) or lower chamber (open circles) fillings for suspension length $l = 2.0$ m.

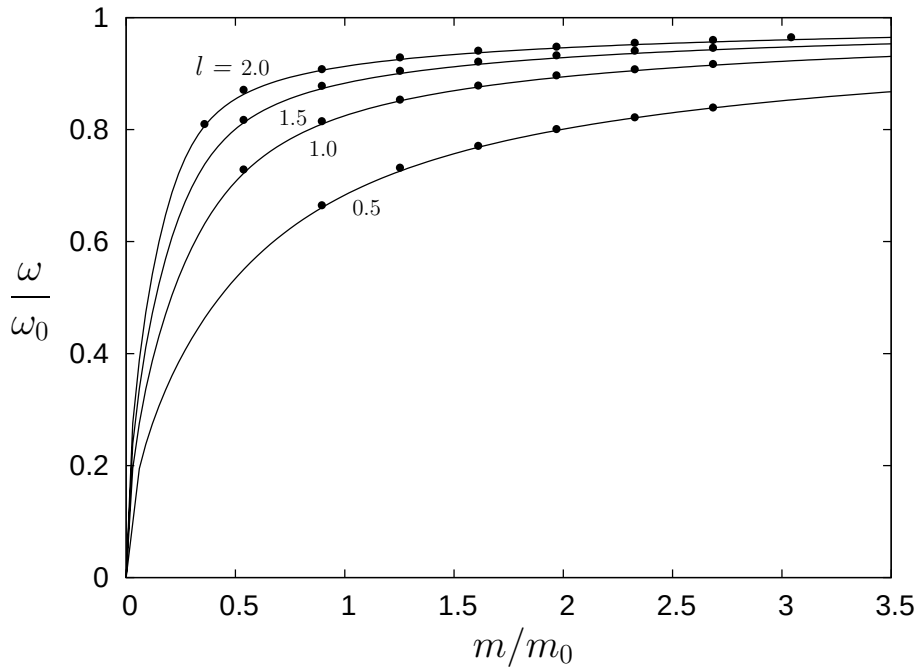

Figure 9. Measured oscillation frequencies of the two-chamber box as a function of m/m_0 for pendulum lengths $l = \{0.5, 1.0, 1.5, 2.0\}$ m using upper chamber fillings. The pendulum lengths l appear in the corresponding dimensionless parameters $\mu = \{0.257, 0.513, 0.770, 1.026\}$.

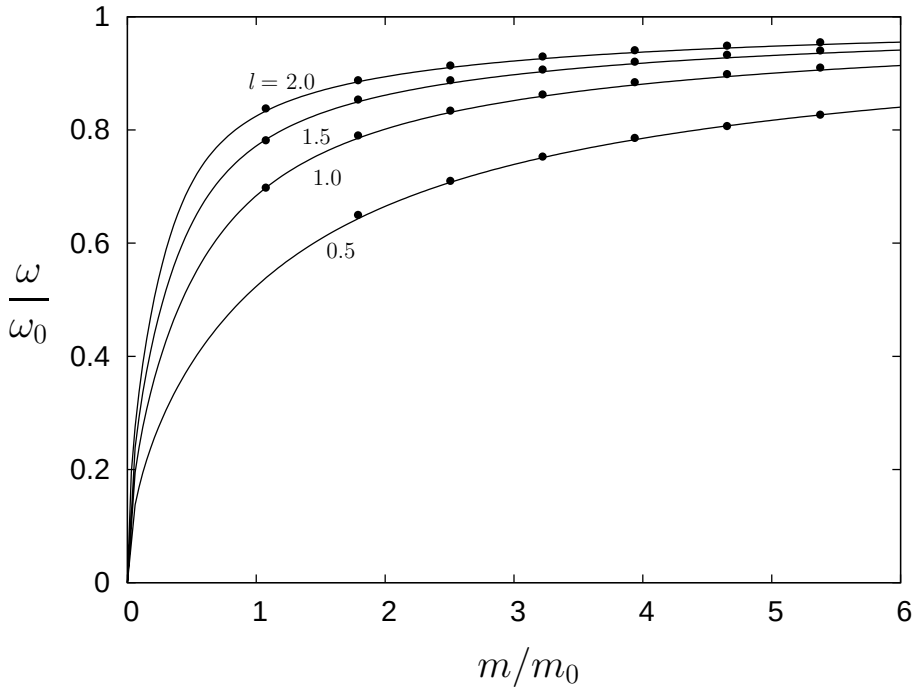

Figure 10. Measured oscillation frequencies of the two-chamber box as a function of mass ratio m/m_0 filled with equal fluid volumes in each chamber for pendulum lengths $l = \{0.5, 1.0, 1.5, 2.0\}$ m. The pendulum lengths l appear in

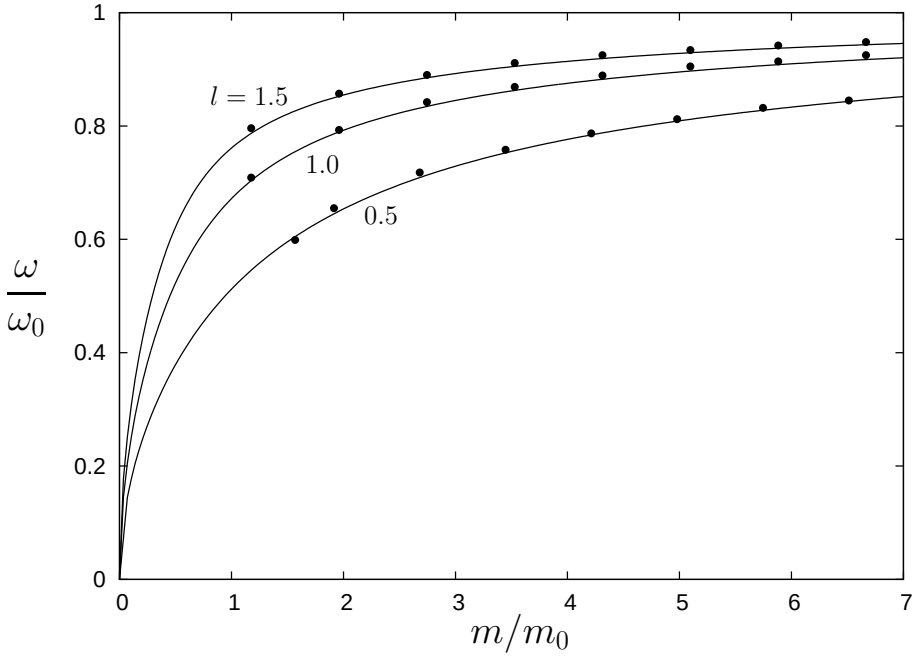

Figure 11. Measured oscillation frequencies of the three-chamber box as a function of mass ratio m/m_0 filled with equal fluid volumes in each chamber for pendulum lengths $l = \{0.5,\ 1.0,\ 1.5\}$ m. The pendulum lengths l appear in the corresponding dimensionless parameters $\mu = \{0.364, 0.728, 1.092\}$.

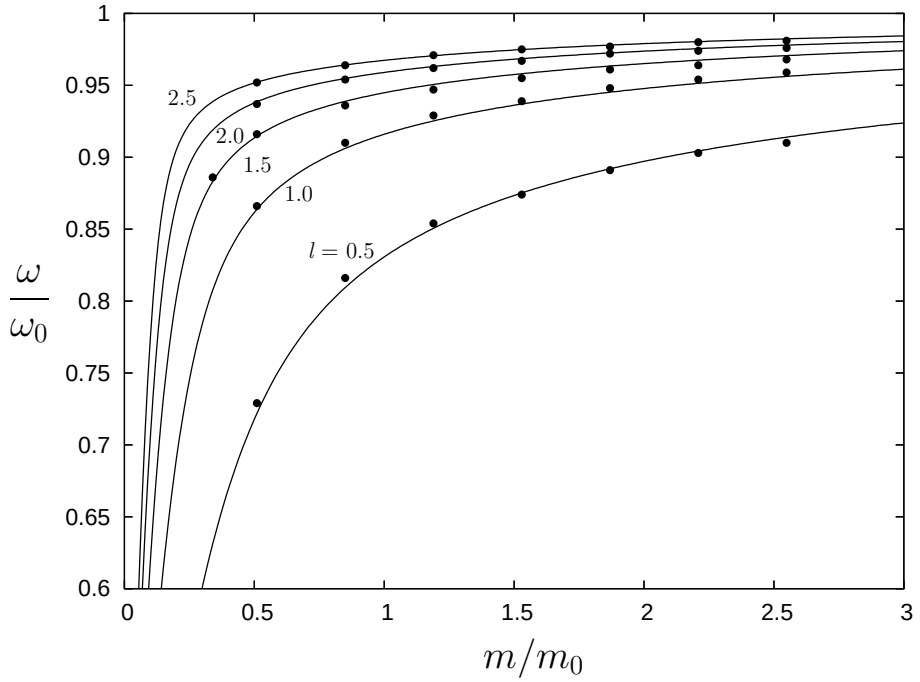

Figure 12. Measured oscillation frequencies of a suspended cylinder as a function of the mass ratio m/m_0 at pendulum lengths $l = \{0.5,\ 1.0,\ 1.5,\ 2.0,\ 2.5\}$ m. The pendulum lengths l appear in the corresponding dimensionless parameters

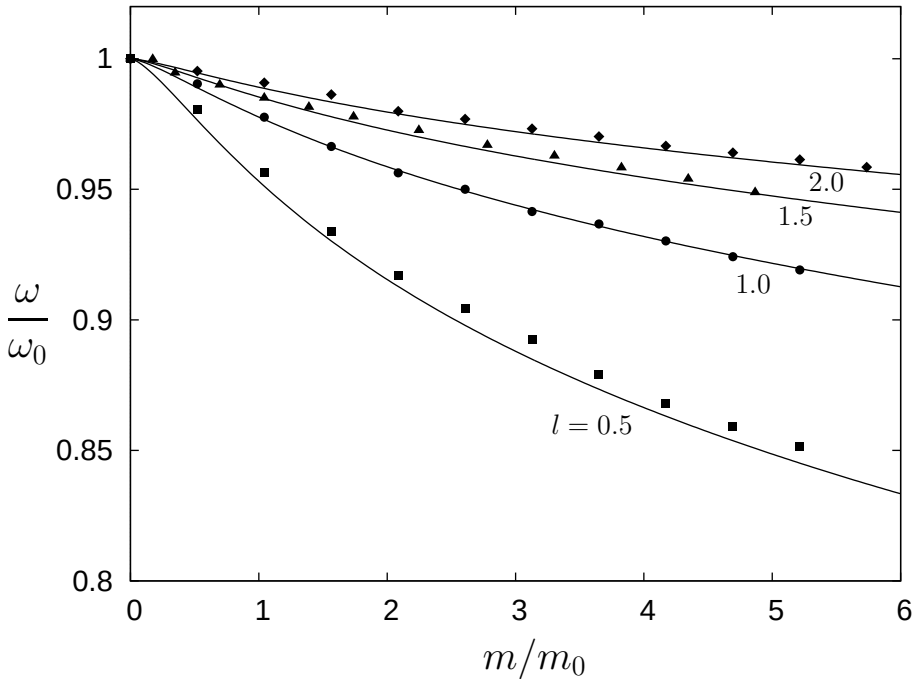

Figure 13. Measured oscillation frequencies for a suspended 90° wedge as a function of mass ratio m/m_0 showing results for pendulum lengths $l = \{0.5,$ 1.0, 1.5, 2.0$\}$ m. The solid lines are from potential theory. The corresponding dimensionless pendulum lengths are $l/H = \{1.640, 3.280, 4.920, 6.560\}$ where H is the height of the wedge given in Table 2.

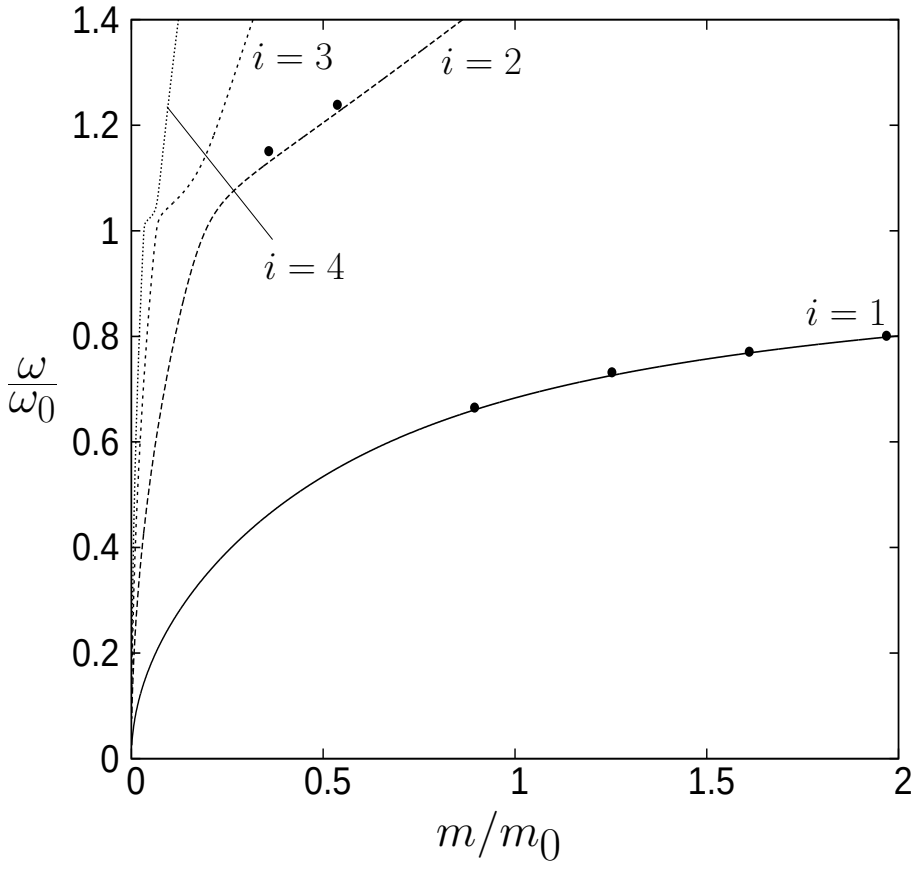

Figure 14. Measured oscillation frequencies for the two-chamber box using the upper chamber only (solid circles) for suspension length $l = 0.5$ m. The lines $i = 1, ..., 4$ represent the normalized oscillation frequencies for the first 4 eigenvalues of (6.1).

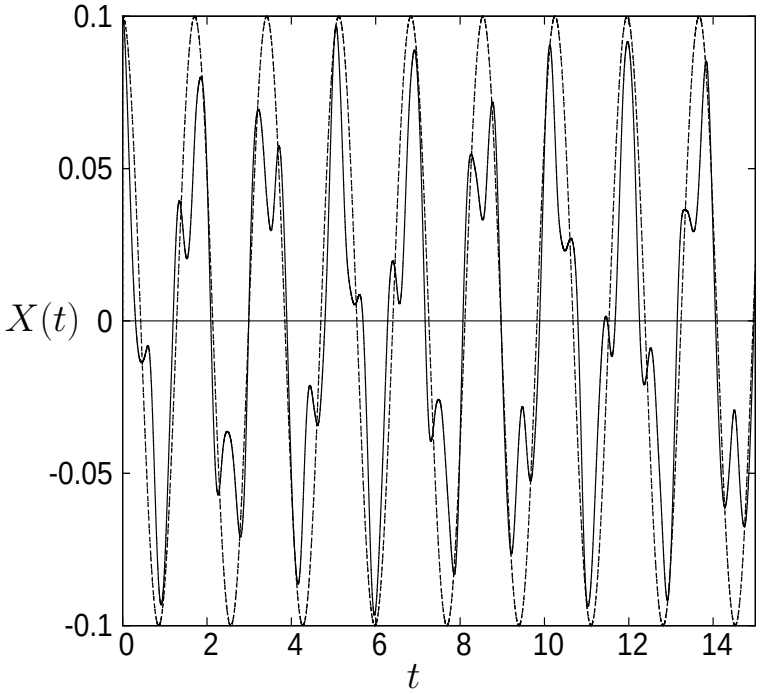

Figure 15a. Simulated vessel displacement $X(t)$ for the two-chamber box using the upper chamber only for suspension length $l = 0.5$ m and $m/m_0 = 2.5$. The dashed line represents the solution containing the 1st eigenvalue of (6.1) only. Here X is measured in meters and t is in seconds.

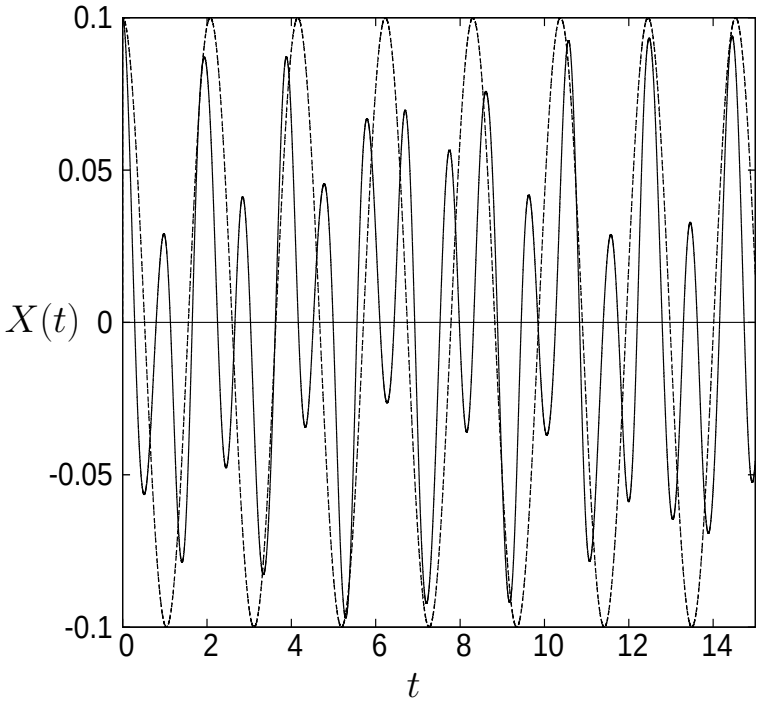

Figure 15b. Simulated vessel displacement $X(t)$ for the two-chamber box using the upper chamber only for suspension length $l = 0.5$ m and $m/m_0 = 1.0$. $X(t)$ is in meters and t is in seconds. The dashed line represents the solution containing

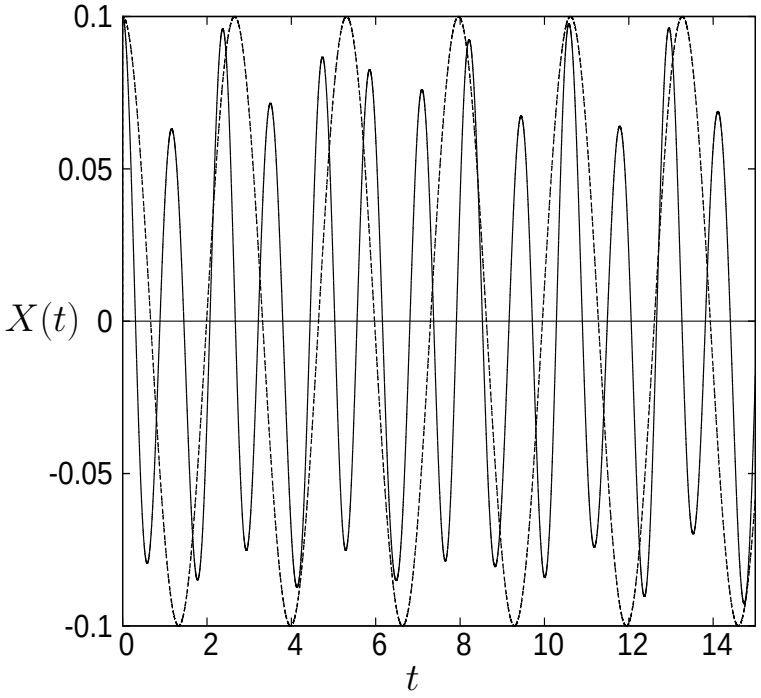

Figure 15c. Simulated vessel displacement $X(t)$ for the two-chamber box using the upper chamber only for suspension length $l = 0.5$ m and $m/m_0 = 0.5$. The dashed line represents the solution containing the 1st eigenvalue of (6.1) only. Here X is measured in meters and t is in seconds.

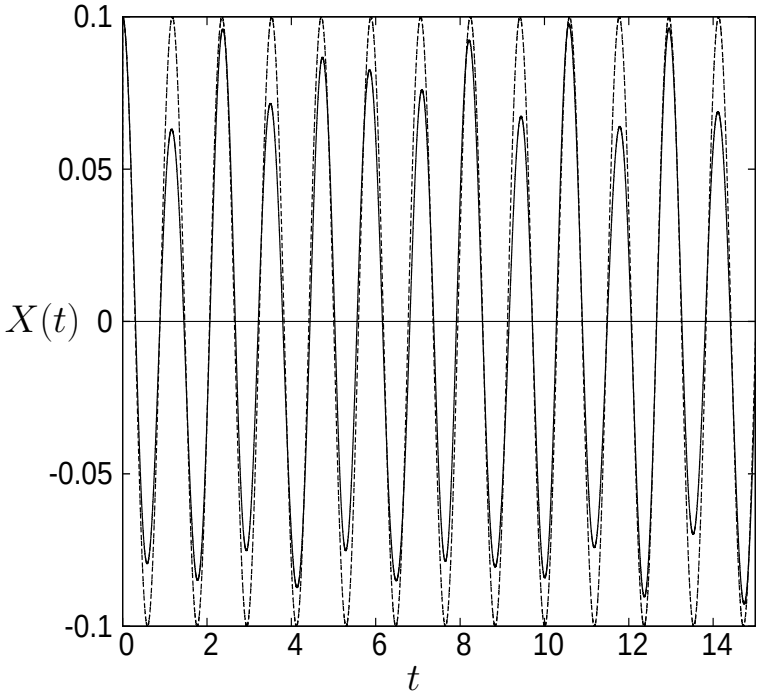

Figure 15d. Simulated vessel displacement $X(t)$ for the two-chamber box using the upper chamber only for suspension length $l = 0.5$ m and $m/m_0 = 0.5$. The dashed line represents the solution containing the 2nd eigenvalue of (6.1) only.

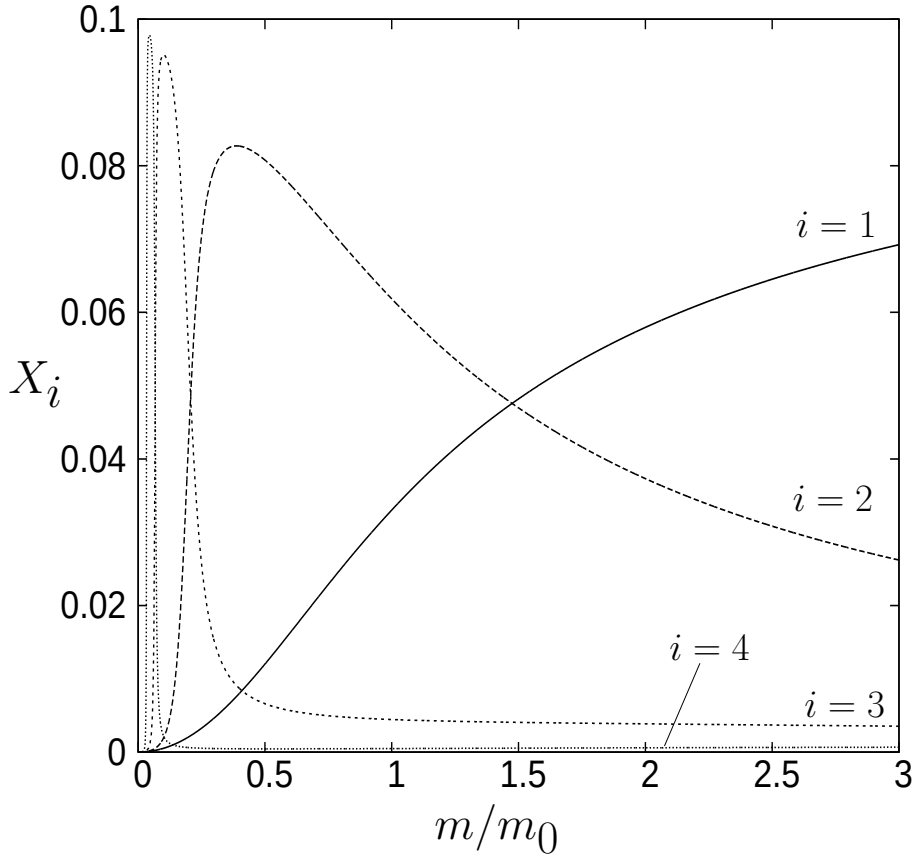

Figure 16. Values of the coefficients of each mode, X_i $(i = 1, ..., 4)$, to satisfy the initial quiescent fluid condition for the two-chamber box using the upper chamber only for suspension length $l = 0.5$ m.

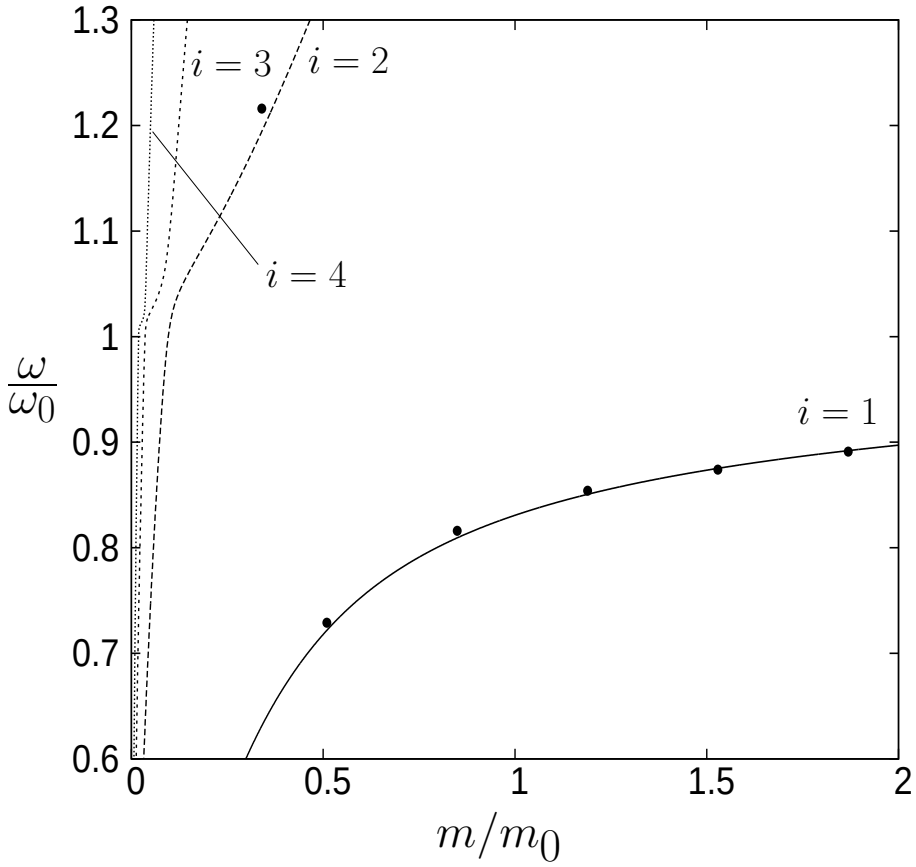

Figure 17. Measured oscillation frequencies for the cylinder (solid circles) for suspension length $l = 0.5$ m. The lines $i = 1, ..., 4$ represent the normalized oscillation frequencies for the first 4 eigenvalues of (3.12a).

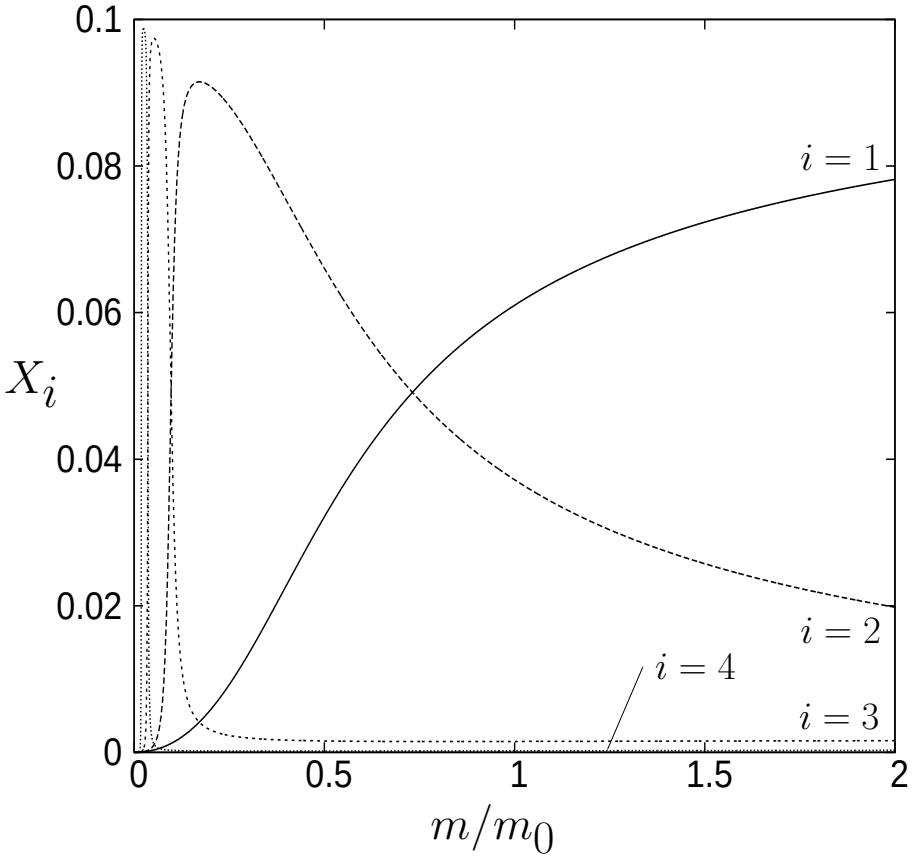

Figure 18. Values of the coefficients of each mode, X_i $(i = 1, ..., 4)$, to satisfy the initial quiescent fluid condition for the cylinder for suspension length $l = 0.5$ m.